Meteorol. Appl. 11, 155–171 (2004) DOI:10.1017/S1350482704001240

On the use of advanced Doppler radar techniques to determine horizontal wind fields for operational weather surveillance

Katja Friedrich & Martin Hagen
Institut fuer Physik der Atmosphaere, Deutsches Zentrum fuer Luft-und Raumfahrt (DLR), Oberpfaffenhofen, Wessling, Germany
Email: Katja.Friedrich@dlr.de, Martin.Hagen@dlr.de

The purpose of this paper is to show how already existing Doppler radar information, provided, for example, by the German Weather Service's (DWD) radar network, can be combined to wind vector fields using multiple-Doppler techniques. At the same time, an alternative to monostatic multiple-Doppler measurements, called a bistatic Doppler radar network, is introduced to measure wind velocity within areas which are not covered by the multiple-Doppler technique or where wind fields close to the earth's surface are required. Advantages, disadvantages, principles and measurement characteristics of the two systems are specified. Additionally, a recommendation is given to arrange each instrument optimally within the network in order to measure wind velocities close to the ground over large areas with high spatial resolution and low error variance. Both systems are applicable either to derive wind fields throughout weather radar networks as shown using the DWD weather radar network, or to act as the basis for weather warning and advisory systems in operation, for instance, at Frankfurt/Main International Airport. Concepts for both applications are given.

1. Introduction

Horizontal winds contribute to the transport of momentum, heat and humidity and are, therefore, an important factor in many meteorological processes. Identifying and analysing severe weather conditions can be supported with the knowledge of temporally and spatially high-resolution wind vector fields. High-quality and rapidly updated wind vector field measurements are required for several applications, especially in regional weather surveillance. Furthermore, the processed wind vector fields can then be assimilated into high-resolution regional numerical weather prediction (NWP) models to further improve weather forecasting. Also, the usage of horizontal wind fields is essential for diagnostic research studies – such as the Mesoscale Alpine Program 1999 (Bougeault et al. 2001; Bousquet & Smull 2003), Improvement of Microphysical PaRameterization through Observational Verification Experiment (IMPROVE) 2001 (Stoelinga et al. 2003), Vertical Exchange and Orography (VERTIKATOR) 2002 (Lugauer et al. 2003) – warning, and nowcasting of severe weather events at airports and around populated areas (e.g. Integrated Terminal Weather System, ITWS, at New York, Orlando, Dallas-Fort Worth, and Hong Kong airport). By deriving rotation, divergence and wind shear pattern from three-dimensional wind fields, flow phenomena (e.g. downslope flow, flow blocking) and local wind systems can be characterised to a higher degree.

Typically, Doppler radar systems sample Doppler velocity and reflectivity over a horizontal range of up to 250 km, with a spatial resolution of a couple of hundred metres and a temporal resolution within minutes. With a traditional monostatic Doppler radar system, only one wind component out of three can be measured. One reason to prefer the use of three-dimensional wind vector fields over one dimensional is the rapid and easy detection of signatures in the wind field, especially for users with little or no experience in interpreting Doppler velocities. Various techniques for scientific and operational use can be applied to retrieve wind vector fields from Doppler velocity and reflectivity measurements of single radars; for example, analytical methods such as Velocity Azimuth Display, VAD (Lhermitte & Atlas 1961; Browning & Wexler 1968), Volume Velocity Processing, VVP (Easterbrook 1975; Waldteufel & Corbin 1979), tracking of radial velocity pattern (Smythe & Zrnić 1983), uniform wind (Persson & Anderson 1987; Hagen 1989), tracking of reflectivity pattern, TREC (Zawadzki 1973; Tuttle & Foote 1990), or variational analysis methods (e.g. Miller & Strauch 1974; Ray et al. 1978; Ray & Sangren 1983; Sun et al. 1991; Laroche & Zawadzki 1994).

One can also determine wind vectors from measurements directly, when a region is monitored by several monostatic Doppler radars. A multiple-Doppler analysis based on least squares estimation is then applied. Horizontal winds can be estimated by at least two Doppler velocity measurements. Over the years, multiple-Doppler analysis has been performed mainly in field experiments due to the expenses incurred in installation, transport and operational usage.

A more economic alternative to several monostatic Doppler radars is a bistatic Doppler radar network (for a cost estimation see Wurman 1994b). Whereas in monostatic Doppler radar systems the transmitter and receiver are collocated, in a bistatic multiple-Doppler radar network several bistatic receivers are spatially separated and arranged around one monostatic radar system. A bistatic receiver conceived specifically for meteorological applications was developed in 1993 by the National Center for Atmospheric Research (NCAR) in the United States (Wurman et al. 1993; Wurman 1994a,b; Wurman et al. 1995). NCAR has used its bistatic network in several research experiments, for example in Kansas (CASES97) and Washington (IMPROVE 2001). As part of a collaboration between the University of Oklahoma, the NCAR and McGill University in Montreal, Canada, two bistatic receivers have been operating, together with the McGill S-band Doppler radar in the Montreal area, since 1996. In 1998, one bistatic receiver was installed at the Deutsches Zentrum für Luft-und Raumfahrt (DLR) in Oberpfaffenhofen (OP), close to Munich in southern Germany. It was the first bistatic radar system operating at C-band with a magnetron transmitter. Since that time, the network has been augmented by two receivers each equipped with two antennas (for more details see Friedrich 2002). More recently, a bistatic Doppler radar network has been installed at the Communication Research Laboratory (CRL) in Okinawa and at Hokkaido University, Japan. Investigations have been initiated on measurement characteristics within a bistatic Doppler radar system and wind vector field analysis (see for instance Skolnik 1990; de Elia & Zawadzki 2000; Friedrich et al. 2000; Takaya & Nakazato 2002; Satoh & Wurman 2003).

The purpose of this paper is to show how Doppler radar information provided by an existing radar network can be used to determine wind vectors for applications such as assimilating wind fields into NWP models or nowcasting of severe weather. As an example we use the dense radar network of the German Weather Service (DWD). Alternatives to monostatic dual-Doppler measurements in terms of a bistatic application are presented for wind field determination within weather radar networks as well as for the use in weather advisory systems operating at airports. We give an overview of the advantages and disadvantages of both monostatic and bistatic Doppler radar networks. The principle of multiple-Doppler measurements and selecting the optimal arrangements of radar systems are discussed in Section 2. In Appendix A measurement characteristics of bistatic radars are summarised. Although Doppler weather radars have been available for several decades, very few weather services have made full use of Doppler velocities for retrieving information such as horizontal wind field. In Sections 3.1 and 3.2 we introduce a concept for estimating wind-vector fields throughout the weather radar network of the DWD using monostatic and bistatic multiple-Doppler techniques. This paper concludes with a proposal on how horizontal wind fields can be utilised for weather surveillance, for example around Frankfurt/Main International Airport using either monostatic or bistatic multiple-Doppler networks (Sections 3.3 and 3.4).

2. Wind measurements with a multiple-Doppler radar network

2.1. Principle of multiple-Doppler radar measurements

When two or more Doppler radar systems are monitoring the same region, the Doppler velocities can be combined to form a wind vector field. Figure 1a illustrates the principle of a monostatic dual-Doppler radar system. Each transceiver both transmits an electromagnetic wave and receives that part scattered backwards. As a result, Doppler velocities cannot be measured simultaneously by a monostatic multiple-Doppler radar network. Rather, each individual radar system scans according to its own particular strategy and time, and scans in a spherical coordinate system centred round the radar. All Doppler velocities must therefore be merged to a reference time and onto a common coordinate system before a wind synthesis based on least squares estimates can be applied. Interpolating each measurement in time and space can be difficult, especially in cases where weather systems evolve rapidly or contain high wind shear.

However, using a bistatic multiple-Doppler radar system reduces not only the high costs of purchasing and installing the equipment but also the interpolation discrepancies, simply because in this system all Doppler velocity measurements are carried out simultaneously since they are based on just a single source of illumination. In a bistatic multiple-Doppler radar system transmitter and receiver are spatially separated, whereas in a monostatic radar system transmitter and receiver are collocated. Figure 1b shows the principle of a bistatic dual-Doppler radar network. The network consists of the traditional transmitting/receiving Doppler radar system plus one passive receiver which has a broad-beam antenna. One great advantage is that bistatic receivers can supplement transmitting Doppler radar systems already in use.

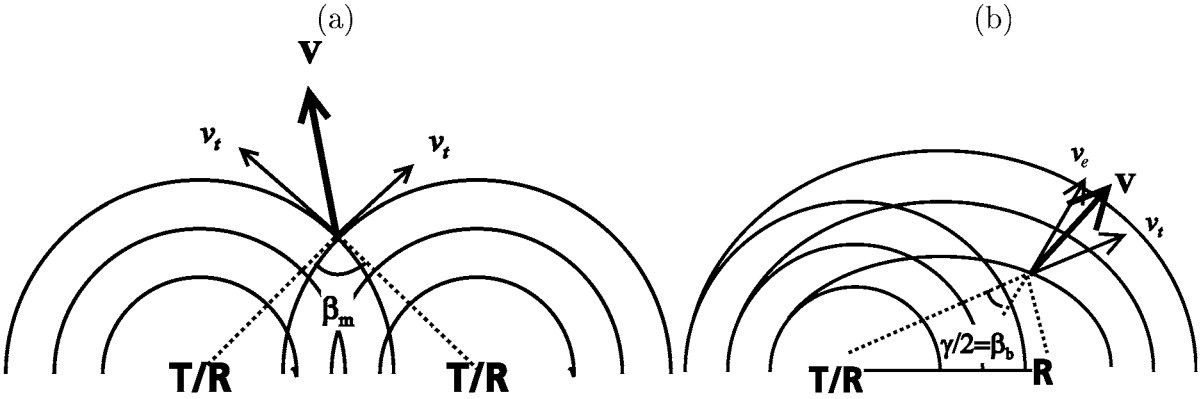

Figure 1. *Schematic view of (a) a monostatic dual-Doppler system consisting of two transceiving radars (denoted as T/R) and (b) a bistatic dual-Doppler system consisting of one transceiver and a passive bistatic receiver located at a remote site (labelled as R). Surfaces of constant time delay are (a) spheres for T/R and (b) ellipsoids for R, respectively. Wind vector V is composed either of (a) two radial velocity components, v_t, or (b) v_t and the velocity component perpendicular to the ellipsoid, v_e, measured by the bistatic receiver. Scattering and intersecting angles are marked. The two-dimensional cross-section is obtained along the scattering plane. More explanation in the text.*

Another considerable advantage is that a bistatic receiver costs less than 5% of a typical weather radar system (Wurman 1994b).

Each bistatic remote receiver consists of an autonomous signal processor integrated into a personal computer and a slotted waveguide antenna having a length of 1.5 m (for C-band radar) and surrounded by a triangular reflector having an edge length of 30 cm (for more details, see Wurman et al. 1995; Friedrich 2002). For measuring during stratiform precipitation events, antennas are used that have a horizontal aperture of 60° and a vertical antenna aperture of 8°, which leads to an antenna gain of 16 dB. For measuring during thunderstorms, antennas with a vertical aperture of about 22° are used, which reduces the antenna gain to 11 dB. Power, Doppler velocity and spectral width are calculated at each signal processor on a gate-by-gate basis. In addition, a central hub computer transmits radar parameters (azimuth, elevation, phase angles and transmitted pulse time) to the remote sites, receives the processed radar data from each receiver and then performs the wind synthesis. Communication between the remote receiver and the central bistatic hub computer can be maintained, for instance via a TCP/IP network based on ISDN communication having a transfer rate of 64 kbits/s.

2.2. Accuracy of wind vector

Apart from the influence of instrumentation effects and meteorological parameters on the accuracy of each wind field measurement, the accuracy of measuring the horizontal wind field is also affected by the angle intersecting the two measured Doppler velocity components. The process of estimating the wind vector is stable numerically only if the intersecting angle is large enough so that two independent components of the wind are available. What now follows is a more detailed discussion of the intersecting angle and its impact on the accuracy of wind vector estimation.

In a monostatic multiple-Doppler installation, the radial velocities measured by each individual monostatic Doppler radar are combined to a wind vector. The unit vectors of two radial velocities intersect at an angle called the intersecting angle, β_m (Figure 1a). Davies-Jones (1979) has demonstrated the error variances σ_u^2 and σ_v^2 of the velocity component in x–direction u and in y–direction v. Error variances are related to the Doppler mean velocity variances of two individual radars, σ_1^2 and σ_2^2, by

$$\frac{\sigma_u^2+\sigma_v^2}{\sigma_1^2+\sigma_2^2} = \sin^{-2}(\beta_m). \qquad (1)$$

In the following discussion, the standard deviation of the wind velocity measurement at a monostatic or bistatic receiver is assumed to be 0.8 m s^{-1} ($\sigma_1 = \sigma_2$). The dependency of the standard deviation on the horizontal wind derived by a monostatic dual-Doppler system, $\sigma^{mo}_{|V_b|}$, on β_m is exhibited in Figure 2 (dashed line). An upper limit of $\sigma^{mo}_{|V_b|} \leq 3$ m s^{-1} leads to an intersecting angle limit ranging between about 20° and 160°. Figure 3a illustrates the spatial distribution of $\sigma^{mo}_{|V_b|}$ at ground level. The areal coverage is about 47 490 km^2 for a radar separation of 30 km. In Figure 3a an intersecting angle limit of 20°–160° corresponding to $\sigma^{mo}_{|V_b|} \leq 3$ m s^{-1} is marked as a thick black line. The minimum value of $\sigma^{mo}_{|V_b|} = 1.1$ m s^{-1} is reached at $\beta_m = 90°$. If β_m approaches 0° or 180°, respectively, $\sigma^{mo}_{|V_b|}$ becomes infinite (cf. Figure 2, Figure 3a).

For a bistatic dual-Doppler radar system, the horizontal wind vector consists of v_t and v_e (cf. Figure 1). In

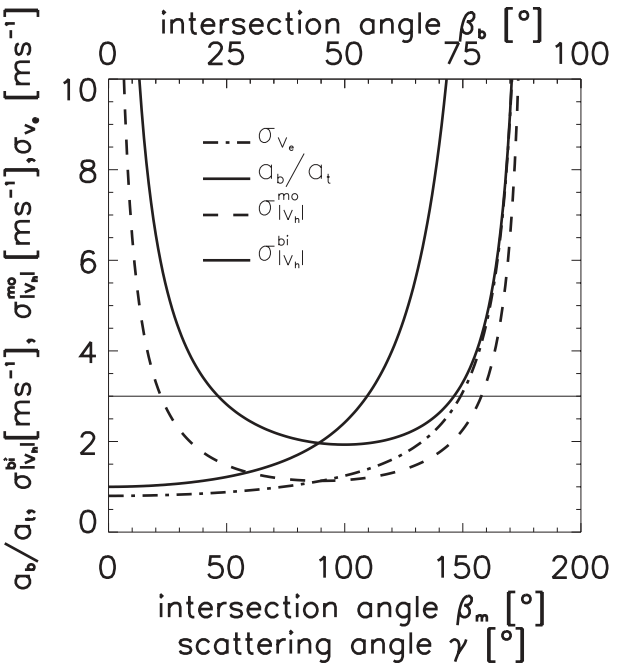

Figure 2. *Illustration of the dependency of the bistatic resolution volume length normalised by the monostatic one, a_b/a_t, the standard deviation of the bistatically measured wind component, σ_{V_e}, the standard deviations of the horizontal wind field measured by a monostatic dual-Doppler system, $\sigma^{mo}_{|V_h|}$, and a bistatic dual-Doppler system $\sigma^{bi}_{|V_h|}$ on the scattering angle (γ) and the respective intersecting angles, β_m, β_b. The standard deviation of the Doppler velocity measurement of the monostatic and bistatic receiver is assumed to be 0.8 m s^{-1}.*

this case the intersecting angle, β_b, is identical to $\gamma/2$. Analogous to Eq. 1 and as demonstrated by (Takaya & Nakazato (2002) and Satoh & Wurman (2003), the error variance σ_u^2 and σ_v^2 of the velocity component can be written as

$$\frac{\sigma_u^2+\sigma_v^2}{\sigma_1^2+\sigma_2^2}=\frac{2(\cos^2(\beta_b)+1)}{\sin^2(2\,\beta_b)}. \qquad (2)$$

The dependency of both the standard deviation of the horizontal wind derived by a bistatic dual-Doppler system, $\sigma^{bi}_{|V_h|}$, on β_b and its spatial distribution are illustrated in Figures 2 and 3b, respectively. A minimum of $\sigma^{bi}_{|V_h|}=2.2$ m s^{-1} within the bistatic dual-Doppler network is reached at $\beta_b=50°$ (Figure 2). If the intersecting angle, β_b, approaches 0° or 90°, respectively, $\sigma^{bi}_{|V_h|}$ becomes infinite. When setting the upper limit of $\sigma_{|V_h|}=3$ m s^{-1}, as in the monostatic dual-Doppler case, the intersecting angle limit becomes $25°\le\beta_b\le75°$ (thick line marked in Figure 3b). Owing to $\beta_b=\beta_m/2$ and the limited horizontal antenna aperture of 60° (for more details see Section 2.4), notice that the bistatic dual-Doppler coverage area is about one-tenth of the monostatic coverage area. However, by installing two bistatic antennas per receiver, the size of the observation area can then be doubled as indicated in Figure 3b.

2.3. Optimal arrangement of monostatic radar systems

Estimating wind vector field by using monostatic multiple-Doppler radar systems has been performed for more than 30 years, for example by Bohne & Srivastava (1976), Ray et al. (1978, 1980) and Ray & Sangren (1983). The early findings of the basic work were summarised at a workshop on how to operate monostatic multiple-Doppler radar systems (Carbone et al. 1980).

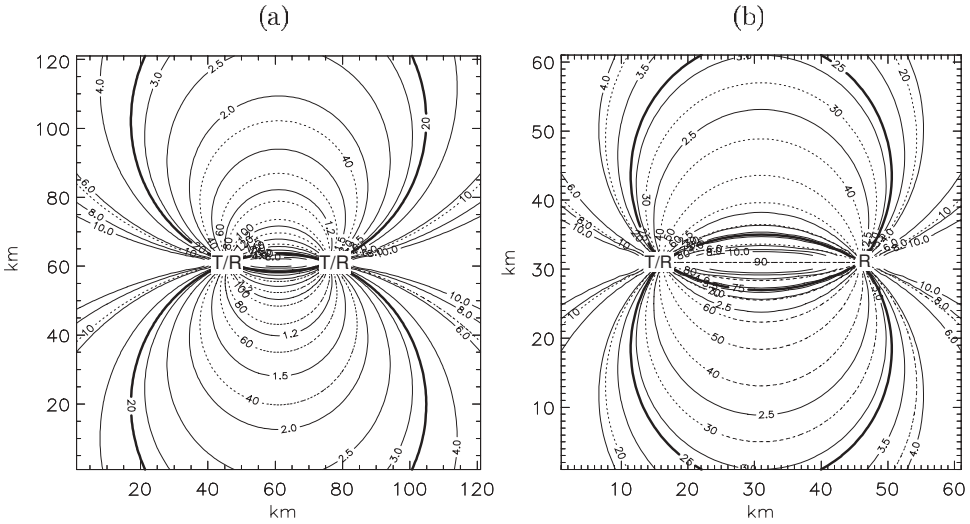

Figure 3. *Spatial distribution of the $\sigma_{|V_h|}$ (thin solid lines) at ground level for (a) a monostatic dual-Doppler radar network and (b) a bistatic dual-Doppler radar network. The separation between the two transceivers (denoted as T/R) and transceiver/bistatic receiver (denoted as R) is 30 km, respectively. Note that the maximum contour line is set at a value of ten. The intersecting angles, β_m and β_b, are marked in dotted lines, respectively. The intersecting angle limit of (a) $20°\le\beta_m\le160°$ and (b) $25°\le\beta_b\le75°$ is shown as thick solid lines.*

Davies-Jones (1979) showed that the optimum spacing between two radars is influenced by measurement error, areal coverage and spatial resolution. Generally, the effectiveness of the dual-Doppler coverage decreases in direct proportion to the increasing distance owing to the spatial resolution becoming gradually less refined and the lowest observation level unacceptably high for increasingly larger parts of the area covered (Davies-Jones 1979). For instance, at a range of 100 km from the transceiver, the resolution volume has a width of about 2 km for an antenna with 1° beamwidth. At this distance, the first radar echo is expected at a height of 2.3 km above radar height level 'accounting for the earth's curvature', making horizontal divergences near the earth's surface impossible to detect.

The optimal radar distance depends largely on the phenomena under investigation, which in turn determine the desirability of whether to compromise spatial resolution in favour of larger coverage. Davies-Jones (1979) proposed that an optimal distance between two radars would range between 43 km and 81 km for an accuracy of between 2 $\mathrm{m\,s^{-1}}$ and 4 $\mathrm{m\,s^{-1}}$, and a horizontal resolution on a Cartesian grid would range between 1 km and 1.5 km. Distances between operational radars are usually far more than 100 km. For hydrological applications, the main purpose behind building up a radar network is to achieve a large areal coverage as opposed to a dense one. Construction costs for new radar systems and yearly operational expenses are also reasons for choosing those radar separations. The future will show if radar separation of more than 100 km is also sufficient for applying radar-derived wind vectors, for example nowcasting of severe weather or assimilating radar data into NWP models.

The total coverage area depends not only on the area being defined by the upper limits on velocity error variance, $A_1(\beta_m^{limit})$, but also on the area being defined by maximum range, $A_2(r_{\max})$. The size of both areas is influenced by the radar separation, d.

According to Davies-Jones (1979), the areal coverage depending on d and the upper limits on velocity measuring error defined by intersecting angle limit in radians, β_m^{limit}, is given as

$$A_1\left(\beta_m^{limit}\right) = 2\left(d\,\sin^{-1}\left(\beta_m^{limit}\right)\right)^2 \times \left(\pi - 2\beta_m^{limit} + \sin\left(2\beta_m^{limit}\right)\right). \quad (3)$$

As exhibited in Figure 2, $\sigma_{\mathrm{V}_b}^{mo}$ is symmetrical around the minimum value within a monostatic dual-Doppler configuration, thereby leading to a single upper limit (e.g. $\beta_m^{limit} = 20°$). Dashed lines in Figure 4 represent the areal coverage $A_1(\beta_m^{limit})$ for variable d and $\sigma_{|\mathrm{V}_b|}$. For example, assuming a maximum standard deviation of about 3 $\mathrm{m\,s^{-1}}$, the coverage area, $A_1(\beta_m^{limit})$ amounts to a size of 47490 $\mathrm{km^2}$ for $d = 30$ km.

The maximum area which can be covered by two radars at an elevation of 0° is given by Davies-Jones (1979) as

$$A_2(r_{\max}) = 2r_{\max}^2\left(\cos^{-1}\left(\frac{d}{r_{\max}}\right) - \frac{d}{r_{\max}}\left[1 - \frac{d^2}{r_{\max}^2}\right]^{0.5}\right), \quad (4)$$

where $r_{\max}$ is the maximum range of the transceiver. Note that with increasing elevation, $A_2(r_{\max})$ decreases. The dual-Doppler area is now defined as the area common to both $A_1(\beta_m^{limit})$ and $A_2(r_{\max})$. The complex shape of the common area can be computed numerically (more details in Davies-Jones 1979).

Both scanning time and mode of each Doppler radar within a multiple-Doppler network have to be synchronised (Ray et al. 1979). Ambiguities can be reduced by using only those radars sophisticated enough to have both a large number of range gates and fast scanning antennas of small beamwidth (Ray et al. 1979).

2.4. Optimal arrangement of bistatic radar systems

Analogous to a monostatic dual-Doppler radar network, the total areal coverage depends also on the area defined by the limits on standard deviation, $A_1(\beta_b^{li1}, \beta_b^{li2})$, and on the area defined by maximum range, $A_2(n_{rb})$. The areal coverage for an elevation angle of 1° depending on the distance between transceiver and bistatic receiver, b, and the upper limit of standard deviation as defined by β_b^{li1} and β_b^{li2} can be calculated as

$$A_1\left(\beta_b^{li1}, \beta_b^{li2}\right) = \left(\frac{b}{\sin\left(\beta_b^{li1}\right)}\right)^2\left(\pi - \beta_b^{li1} + 0.5\sin\left(2\beta_b^{li1}\right)\right) - \frac{r^2}{2}\left(\pi - \beta_b^{li2} - \sin\left(\beta_b^{li2}\right)\right), \quad (5)$$

where

$$r = \frac{b\sin\left(\beta_b^{li2}/2\right)}{\sin\left(\pi - \beta_b^{li2}\right)}.$$

This calculation is based on reception using only one bistatic antenna having a horizontal antenna aperture of 60° (Figure 3b, upper part). If two bistatic antennas are installed at one bistatic receiver (this can be automatically selected according to the azimuth angle of the transmitting radar beam), the size of the coverage area doubles (Figure 3b, upper and lower part). The coverage area, $A_1(\beta_b^{li1}, \beta_b^{li2})$, using a bistatic dual-Doppler radar equipped with one antenna depending on $\sigma_{|\mathrm{V}_b|}$ and b, is illustrated in Figure 4 by solid lines. Compared to a monostatic dual-Doppler arrangement, the number of bistatic receivers has to be increased by ten (theoretically at least) in order to be able to observe

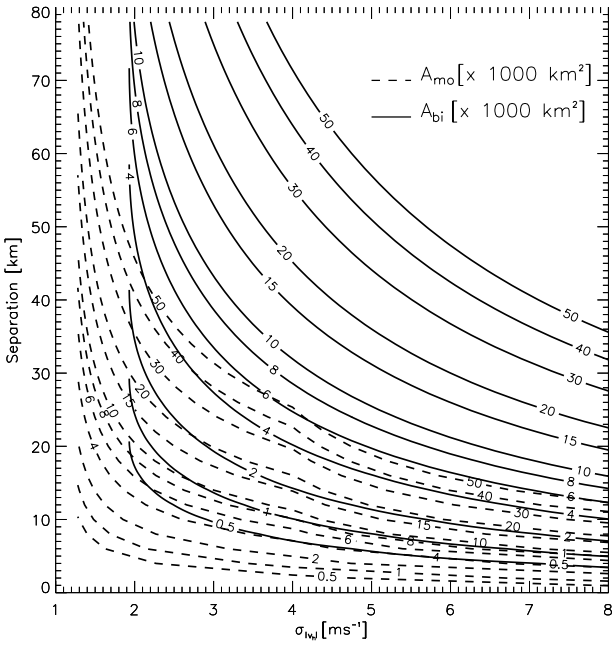

Figure 4. *Coverage area, A_1, for a monostatic (dashed lines) and bistatic (solid lines) dual-Doppler radar network depending on both the standard deviation of the horizontal wind vector determination, $\sigma_{|V_b|}$ and the distance between transmitter and bistatic receiver. The coverage area is labelled in 1000 km² and ranges between 500 km² and 50000 km².*

an area of equal size where $d = 30$ km. When each receiver is equipped with two antennas, the number reduces to five bistatic receivers. Even five receivers together makes a total cost of only about 25% of a Doppler weather radar and are therefore still less expensive than installing a second monostatic Doppler radar for dual-Doppler application.

The size of the area under observation can be defined not only by the viewing angle of the bistatic antenna and $A_1(\beta_b^{li1}, \beta_b^{li2})$, but also by combining the size of the maximum range (maximum sample ellipsoid) together with the distance between receiver and transmitter. The resulting maximum sample ellipsoid is a function of the sample spacing measured in seconds, τ_s, and the number of range-gates, n_{rb}. The latter is limited due to the bandwidth in the data transfer between the remote receiver and the central hub computer.

The signal, when measured by the bistatic receiver at a given time, is referred to an ellipsoid of constant delay, which includes all signals having the same propagation time. Therefore, the maximum area which can be covered by a bistatic dual-Doppler radar system is

$$A_2(n_{rb}) = \pi\,(0.5\tau_s\, c\, n_{rb} + b)((0.5\tau_s\, c\, n_{rb} + b)^2 - 0.25b^2). \quad (6)$$

Since n_{rb} and b are usually fixed, $A_2(n_{rb})$ can be enlarged by increasing τ_s.

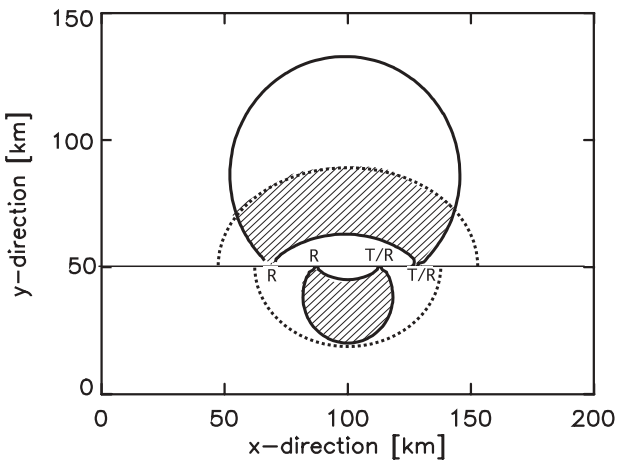

Figure 5. *Schematic view of the maximum sample areas corresponding to a baseline length of 60 km (upper part) and to a baseline length of 30 km (lower part). This estimation is limited by an intersecting angle limit of 25°–75° (solid line) for both applications. The maximum sampled ellipses assumed are shown by dotted lines. The resulting observation areas are cross-hatched.*

Figure 5 shows schematically the dependency of $A_1(\beta_b^{li1}, \beta_b^{li2})$ and $A_2(n_{rb})$ on the total coverage area. Here, the main axis of the maximum sample ellipsoid has a length of $b + 45.70$ km with $b = 60$ km (upper part) and $b = 30$ km (lower part). The maximum sample ellipsoid is indicated by the dotted line (radar parameters are related to the DLR system with $\tau_s = 1.25\,\mu$s, $n_{rb} = 126$). The intersecting angle limit of $25° \le \beta_b \le 75°$ ($\sigma_{|V_b|} \le 3$ m s^{-1}) is delineated by thick lines. Therefore, the investigation area (cross-hatched) is restricted either by the intersecting angle limit, $\beta_b^{li1}, \beta_b^{li2}$ (Fig. 5, lower part) or by increasing b the maximum ellipsoid (Fig. 5, upper part). A large separation between transceiver and receiver leads to a large $A_1(\sigma_{|V_b|})$. The upper part of Figure 5 shows that, if the maximum range does not increase adequately, the observation area is not used to best advantage.

The area totally covered when $b = 60$ km is larger than the one achieved when $b = 30$ km, including the area with high accuracy in the horizontal wind field determination the outer edge where $\beta_b = 50°$. Note that when $b = 60$ km at a 1° elevation, measurements from the transceiver are possible only above a radar height level of 1 km at a distance of 50 km, and above 1.8 km at a distance of 80 km. Furthermore, as the distance from the transceiver increases so the size of the sample volume increases proportionally, the results of beam-broadening. A wind field close to the ground can yield important information regarding weather development. The lack of wind vectors close to the ground can cause inaccurate weather forecasts and vertical wind determination when integrating the continuity equation (boundary effects).

In Table 1, the size of the total area under observation, depending on $A_1(\sigma_{|V_b|})$ and $A_2(n_{rb})$, is tabulated

Table 1. *Areal coverage in km² as a function of receiver–transceiver separation, b, in km (top number); maximum values of $\sigma^{bi}_{|V_b|}$ in m s^{-1} (left number); and resolution volume length, a_b. The upper value of the surface area represents a resolution volume length of 300 m; the middle value of 500 m; and the lower value of 700 m. The bold values mark those configurations where the size of A_1 fits optimally into the size of A_2, while still in the underlined configuration of $A_1 > A_2$. Within all the remaining configurations, the size of A_2 is larger then the size of A_1. Calculations are based on those radar parameters which are related to the DLR system.*

$a_b = 300$ m $a_b = 500$ m $a_b = 700$ m	10 km	20 km	30 km	40 km	50 km
2 m s^{-1}	76	299	690	1215	1906
	76	299	690	1215	1906
	76	299	690	1215	1906
3 m s^{-1}	124	509	1141	2030	3152
	124	509	1141	2030	3171
	124	509	1141	2030	3171
4 m s^{-1}	231	928	2098	*3191*	*4059*
	231	928	2098	3735	5838
	366	1468	3306	5880	9180
5 m s^{-1}	366	1468	*2745*	*3638*	*4453*
	366	1468	3306	5800	*7622*
	366	1468	3306	5880	9180
6 m s^{-1}	551	*2052*	*3069*	*3902*	*4699*
	551	2190	4923	*6965*	*8516*
	551	2190	4931	*8768*	12146

according to the transceiver–receiver separation, the resolution volume length and the upper limit of standard deviation. Values boldly marked indicate an arrangement where $A_1(\sigma_{|V_b|})$ fits optimally into the area of $A_2(n_{rb})$ (Fig. 5, lower part). The values underlined represent a configuration where $A_2(n_{rb}) < A_1(\sigma_{|V_b|})$ (Fig. 5, upper part). Optimal distance between transceiver and bistatic receiver depends on required accuracy and range resolution. For instance, when requiring an accuracy of lower than 3 m s^{-1} in the horizontal wind, the distance should range between 20 km and 30 km for a range resolution of 150 m (values not shown in Table 1), between 40 km and 50 km for a range resolution of 300 m, and between 60 km and 70 km for a range resolution of 700 m (values not shown in Table 1).

3. Future application

3.1. Wind vector fields throughout the weather radar network of DWD using monostatic multiple-Doppler techniques

The DWD has built up a network of 16 C-band weather radar systems. Volume scans are performed every 15 minutes with 18 elevations ranging between 0.5° and 37°. The maximum range is 240 km for the intensity

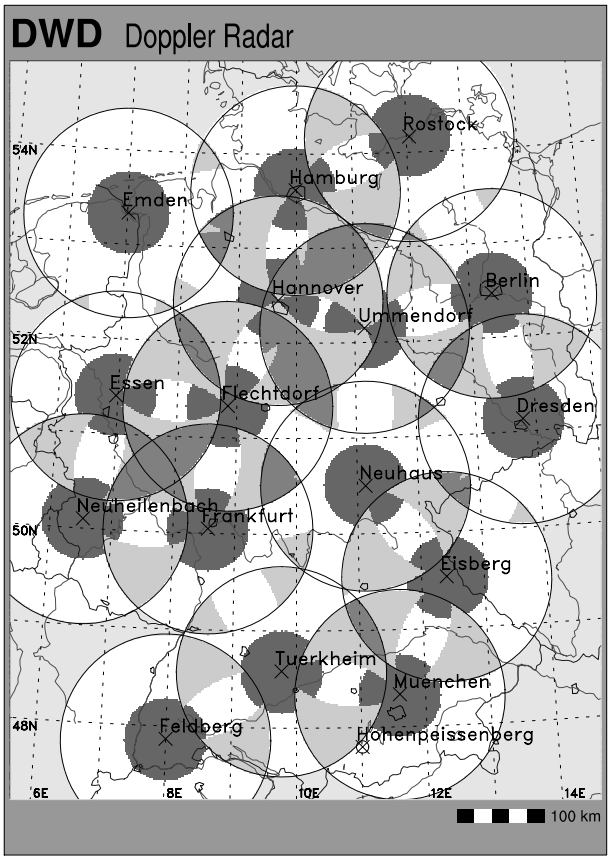

Figure 6. *Map of a possible horizontal wind coverage in Germany using Doppler weather radar information provided by the Deutsche Wetterdienst. Each monostatic weather radar, together with the 125 km ranges of Doppler measurements, are displayed as black circles. Areas shown in light grey illustrate monostatic dual-Doppler radar coverage. Grey areas mark where the horizontal wind field can be determined when using at least three independent wind components. Dark grey patches represent areas having a radius of 50 km and indicate the dual-Doppler areas of the bistatic network. The monostatic multiple-Doppler areas are restricted to an intersecting angle limit of 20° to 160°.*

mode and 125 km for the Doppler mode. Figure 6 illustrates the weather radar location and the 125 km maximum range ring. Reflectivity, Doppler velocity and spectral width are sampled operationally every 15 minutes. The DWD precipitation and Doppler products are derived from this volume data. In addition to volume scans, precipitation scans with a maximum range of 125 km are performed at an elevation between 0.5° and 1.8° every 5 minutes. One can estimate the quantitative precipitation rate from precipitation scans. A detailed description of the DWD radar network, including radar specifications, quality-control of radar data, and DWD radar products, can be found in Schreiber (1998). The radar system located on Mount Hohenpeissenberg is operated as a research radar and does not contribute to the operational network and radar composite.

Figure 6 shows that when volume scans are performed, horizontal wind fields can be determined by measuring

Table 2. *Table of the possible dual-Doppler combinations within the DWD radar network listing radar separation distances, differences in radar heights in m (relative to the first-named radar), and beam height ($\Delta h + H$) at a distance of 100 km and 0.5° elevation.*

Combination	Distance (km)	Δh (m)	Beam height (km) where $r = 100$ km, $\phi = 1°$
Türkheim, Eisberg	232.7	−65	1.5
Hanover, Essen	229.6	−99	1.6
Neuheilenbach, Flechtdorf	224	48	1.5
Ummendorf, Dresden	222.7	−45	1.5
Berlin, Rostock	216	45	1.5
Emden, Hanover	211.8	−22	1.5
Dresden Neuhaus	209.1	−285	1.7
Emden, Hamburg	205.7	13	1.5
Frankfurt, Neuhaus	199.5	−369	1.8
Frankfurt, Essen	197.4	−34	1.5
Türkheim, Frankfurt	196.2	585	2.0
Flechtendorf, Neuhaus	194.3	17	1.5
Ummendorf, Neuhaus	192.4	−330	1.8
Flechtdorf, Ummendorf	191.9	347	1.8
Ummendorf, Hamburg	188.2	139	1.6
Türkheim, Feldberg	163.7	−775	2.2
Berlin, Ummendorf	161.1	−105	1.6
Berlin, Dresden	157.7	−150	1.6
Essen, Neuheilenbach	155.3	400	1.9
Munich, Eisberg	154.9	−281	1.7
Rostock, Hamburg	153.3	−11	1.5
Frankfurt, Neuheilenbach	153.2	−434	1.9
Frankfurt, Flechtendorf	151.6	−386	1.8
Eisberg, Neuhaus	148.3	281	1.7
Munich, Türkheim	147.2	514	2.0
Flechtdorf, Hanover	142.8	451	1.9
Flechtdorf, Essen	137.1	352	1.8
Hanover, Hamburg	136.1	35	1.5
Ummendorf, Hanover	110.6	104	1.6

wind samples taken from two or three independent Doppler radar systems within the overlapping areas, illustrated as light grey or grey areas, respectively. The area of horizontal wind field determination is limited by an error variance of 3 m s^{-1}, indicated by an intersecting angle limit of 20° and 160°. Note that all radar systems are Dopplerised (see http://www.dwd.de/de/wir/Geschaeftsfelder/Hydrometeorologie/a_href_pages/RADOLAN/radarverbund.htm). The radar network has been established to cover Germany with radar information for hydrological purposes. As a result, the radar separation averages about 180 km and the overlapping areas are limited. The distances between two radar systems range from 111 km for the radars at Hanover and Ummendorf to a distance of 233 km for the radar systems at Türkheim and Eisberg (Table 2). As the distance from the radar increases, so do both resolution volume and the beam height. For instance, at a range of 100 km, the resolution volume has a width of 1.8 km for a beamwidth of 1°. At this distance, the first radar echo can be sampled at a height of 2.3 km above radar height (allowing for the earth's curvature) for an elevation of 1°. When two radars are located at different height levels, radar echoes can first be detected at a height of ($\Delta h + H$). In this case, Δh is the height difference between two radars and H the beam height of the radar which is located at a higher level above mean see level (MSL).

Table 2 shows the radar separation, the height difference, and the beam height ($\Delta h + H$) at a distance of 100 km and at 0.5° elevation for all dual-Doppler radar combinations within the DWD radar network. Within the DWD radar network, high resolution close to the ground can be achieved when using the radar combinations at Hanover and Ummendorf, Hanover and Hamburg, and Rostock and Hamburg. In some areas, the radar separation is sufficient to determine horizontal winds even when using multiple-Doppler techniques (grey areas shown in Figure 6). With overdetermination of the system of the equations for calculating the wind field, $\sigma^{mo}_{|v_b|}$ then reduces. Erroneous wind measurements are then detectable when applying a quality-control scheme devised by Friedrich & Hagen (2004).

One example of the wind field estimation using radar at Türkheim and the DWD research radar at

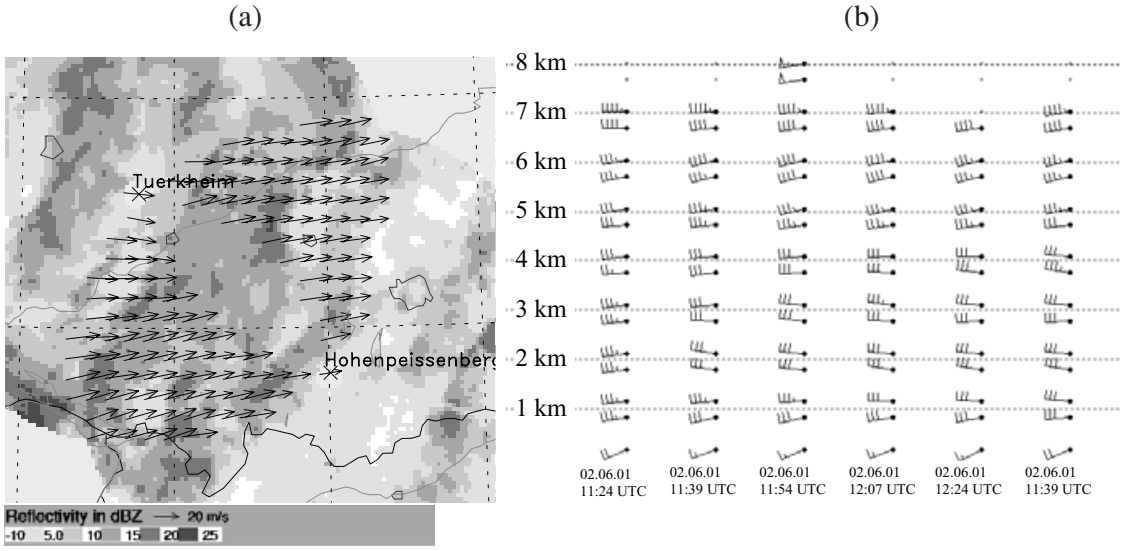

Figure 7. *Example of a horizontal wind field estimation: (a) a horizontal cross-section of dual-Doppler derived horizontal wind field performed at 3 km above MSL at 1156 UTC on 2 June 2001 using radars at Türkheim and at Hohenpeissenberg, and underlaid by the reflectivity factor. For clarity of display, the wind vectors are plotted every 10 km. The wind vector located at the radar site is derived from the vertical profile in (b). (b) represents a vertical profile of the horizontal wind above radar Türkheim sampled between 1124 UTC and 1239 UTC on 2 June 2001. Both data sets were kindly provided by the DWD.*

Hohenpeissenberg (denoted as a cross within a circle in Figure 6) is given in Figure 7a for stratiform precipitation occurring at 1156 UTC on 2 June 2001. Before applying dual-Doppler analysis, both radial velocity fields are interpolated onto a Cartesian grid having a horizontal resolution of 2 × 2 km and a vertical resolution of 1 km. The difference in height between the two radars is 274 m. Each radar system starts scanning more or less at the same time, so that time differences of less than 10 min are negligible during stratiform precipitation events.

It is also possible to detect the vertical profiles of the horizontal wind field occurring above each radar system in addition to dual-Doppler derived horizontal wind fields. For that purpose the VAD technique is applied to radial velocities measured at a scanning elevation of 20°. Figure 7b gives an example of the temporal evolution of the horizontal wind above the radar at Türkheim. Both the wind velocity and the direction up to a height of 8 km are determined every 15 min between 1124 UTC and 1239 UTC on 2 June 2001. The maximum height depends strongly on the availability of scatterers. In clear air C-band radars are able to detect signals up to a height of 1–2 km above the radar. However, within precipitation systems, the measurement increases to a height of 10 km.

For the regions remaining without any dual-Doppler information (shown as white areas in Figure 6), single-radar wind field retrieval can be applied. Hagen (1989) and Hagen et al. (2002) provide detailed information on how to derive horizontal wind fields using different single- and dual-Doppler techniques.

3.2. Wind vector Þelds throughout the weather radar network of DWD using bistatic multiple-Doppler techniques

If each monostatic radar system was equipped with three bistatic receivers, it would be possible to provide wind vector fields with high resolution coverage close to the ground over most of Germany, as illustrated in Figure 6. Dark grey circles representing a radius of about 50 km indicate those areas where horizontal wind vector fields could be estimated using a bistatic radar network. One condition to installing bistatic receivers, however, would be that the weather radars operate with vertical polarisation. Weather radar systems without polarisation diversity normally transmit a horizontally polarised wave because the backscattering cross-section for raindrops is larger than for vertically polarised waves, resulting from raindrops flattening when falling to the ground. In case of hail, the backscattering cross-section is independent of the transmitted polarisation. To determine wind vector fields using bistatic receivers, the monostatic transmitting radar system has to be reconstructed to be able to transmit a vertically polarised wave.

Three bistatic receivers arranged around one monostatic radar offer optimal usage when working with a minimum number of receivers to achieve maximum spatial coverage in horizontal wind field estimations. Within this configuration, the horizontal wind vector fields within a radius of about 50 km around the transmitting radar can be determined with an accuracy of 2–3 m s^{-1}, as illustrated by the cross–hatched areas in Figure 8a.

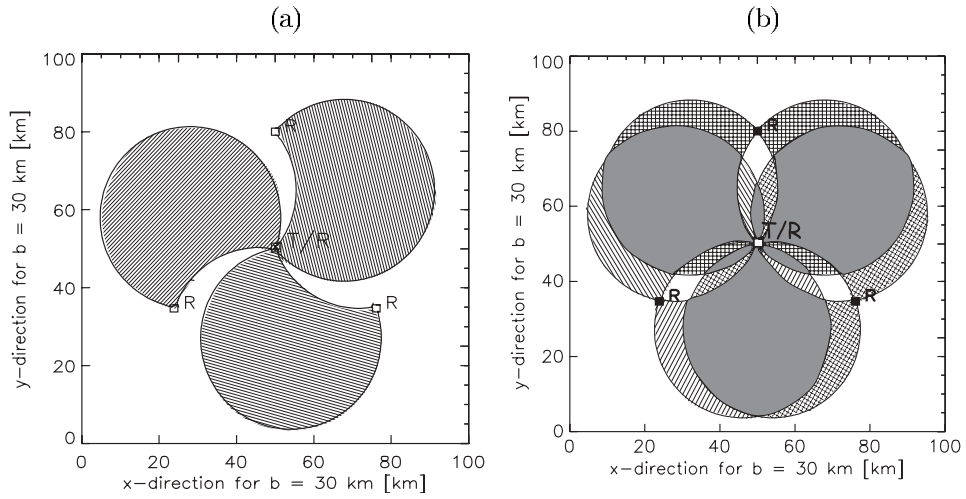

Figure 8. *The horizontal coverage of (a) a dual-Doppler or (b) dual/triple-Doppler processed horizontal wind field. This estimation is limited for both applications by* $25^\circ \leq \beta_b < 75^\circ$. *In (b) each receiver is assumed to be equipped with two antennas. Triple-Doppler areas are marked as grey, dual-Doppler regions are cross-hatched. Hatching corresponds to the respective receiver R.*

The accuracy of the horizontal wind retrieval can be increased to values ranging between 1.5 and 2 $\mathrm{m\,s^{-1}}$ if an additional antenna is installed at each bistatic receiver site which then enables three independent wind components to derive a wind vector as shown by grey areas in Figure 8b. One of two antennas sharing only one bistatic receiver can then be selected automatically according to the azimuth angle of the transmitting radar beam. As indicated in Figure 8b, each antenna has to be carefully positioned in order to cover the intersecting-angle limit of 25° to 75° on both sides of the transmitter–receiver baseline. With this configuration, wind measurements along the transmitter–receiver baseline can be guaranteed through measurements taken by the two neighbouring receivers. Moreover, the equation system used to determine the horizontal wind field components is overdetermined in the grey areas and exactly determined in the cross-hatched areas. Figure 9 illustrates the standard deviation of the horizontal wind for a triple-Doppler application when using one transceiver and three bistatic receivers. The standard deviation of the horizontal wind ranges between 1.5 and 2.5 $\mathrm{m\,s^{-1}}$. Within the overlapping areas, a quality control scheme for horizontal wind fields can be applied (see Friedrich 2002). This scheme includes, for instance, an algorithm dealing with irregularities encountered during measurement, e.g. sidelobe contamination and synchronisation problems between transmitter and receiver.

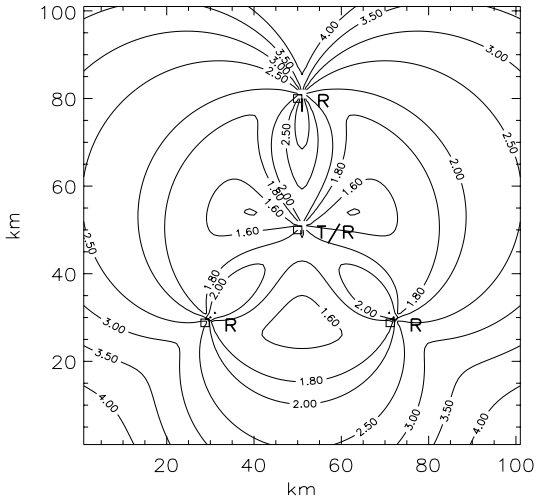

Figure 9. *Spatial distribution of the* $\sigma^{bi}_{|V_b|}$ *in* $\mathrm{m\,s^{-1}}$ *at ground level for a bistatic triple-Doppler radar network. Each receiver is assumed to be equipped with an antenna having an aperture of 360°.*

3.3. Wind vector Þelds in the vicinity of airports using monostatic multiple-Doppler techniques

The distribution of winds in the vicinity of airports impacts on both airport safety and operational efficiency. With knowledge of the wind conditions, runway configurations, aircraft merging, and aircraft separations can be optimised. But knowledge of wind characteristics within the three-dimensional space around the airport is also essential for advisory systems, such as Wake Vortex Advisory Systems which reduces aircraft separation for wake vortex avoidance (Gerz 2001), and the Integrated Terminal Weather System (ITWS) wind-shift and runway-winds prediction system (Cole & Wilson 1994).

When a real-time display of horizontal wind field is combined with reflectivity, severe weather evolution such as convection growth, gust fronts and downbursts can be detected more easily than by relying solely on reflectivity composites or the Doppler velocity field. Convective weather warnings, such as wind shear alerts, can be given immediately. One example of a wind vector display underlaid by radar reflectivity is given in Figure 10, which shows data sampled by the DLR bistatic Doppler radar network during a

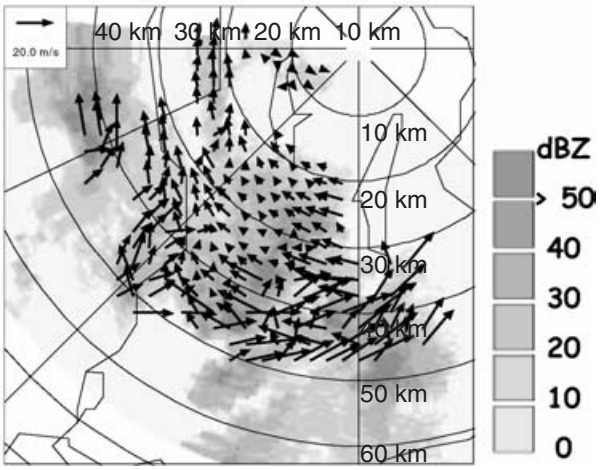

Figure 10. *PPI of wind vector field measured by the DLR bistatic Doppler radar network and underlaid by reflectivity measured by* POLDIRAD *at 5.6° during a downburst-producing thunderstorm passing the observation area at 1600 UTC on 9 July 2002.*

downburst-producing thunderstorm at 1600 UTC on 9 July 2002. The wind field pattern south-southwest of POLDIRAD at a range of 35–45 km can be ascribed to the microburst's early state of development. A microburst was later observed southwest of Munich.

In this section, we suggest how radar information could complement existing ground-based observations in order to cover the terminal area at Germany's most frequented airport, Frankfurt/Main International Airport, with horizontal wind fields within the three-dimensional space. Severe storms are usually associated with precipitation. Precipitation intensity and movement can be monitored by Doppler radar systems with high resolution in both time and space.

In the first concept, an additional C-band Doppler radar (referred to as Frankfurt Doppler radar or FDR) is installed complementary to the already existing C-band radar within the DWD radar network (referred to as network radar). The independent Doppler radar system, FDR, allows rapid-update sector scans or volume scans to maintain a sufficient update (2–5 minutes) to detect wind shear and convective systems. The horizontal wind field can be derived together with the radial velocity measured by the network radar every 15 minutes. The scan algorithm of the FDR can be additionally optimised to reduce scanning time, for example by interlacing scans used by MeteoSwiss radar systems (Joss et al. 1998). Figure 11 illustrates a hypothetical application for determining wind vectors within the terminal approach of the Frankfurt/Main International Airport when combining the network radar with the FDR. The dual-Doppler lobe with an intersecting angle limit of 20° to 160°, shown as a dashed area in Figure 11, covers the terminal approach to runway 25L/25R, marked as black lines. For this application, the existing network radar has to be moved from its present position south of the airport. With a separation of about 35 km between the FDR and the network radar, signatures close to the earth's surface can be detected with a resolution in the order of hundred metres. With this small radar separation, the sensitivity of the receiver is high enough to provide reliable Doppler velocity measurements even in clear-air conditions. Both the areas along the runways and between the radar baseline can be covered by wind measurements achieved, for instance, by a Doppler lidar system, wind profiler, and a ground-based observation station combined with a Low Level Wind Shear Alert System (LLWAS). This arrangement has already been implemented with different sensor equipment at most airports in the USA and Hong Kong.

3.4. Wind vector Þelds in the vicinity of airports using bistatic multiple-Doppler techniques

One alternative to adding another monostatic radar is a bistatic radar network, but this system has not yet been tested operationally. Figure 12 shows a possible configuration of four bistatic receivers installed around the weather radar located at Frankfurt/Main International Airport. In this study, each bistatic receiver is equipped with two antennas, each covering a side of the baseline. One advantage of installing four receivers is that it lowers the margin for error in horizontal wind field determination which arises from overdetermining the system of equations used in calculating the wind field. A second advantage is that the area between the transmitter and receiver baseline, plus the area beyond the bistatic receiver, are always covered by one of the other receivers. Here again, one can see within the overlapping areas that it is possible to apply a quality control scheme for horizontal wind fields (see again Friedrich 2002). Figure 12 illustrates the spatial distribution of $\sigma^{bi}_{|V_h|}$ and minimum detectable reflectivity factor, $Z_{b_{\min}}$ using four bistatic receivers. In the vicinity of the airport, the horizontal wind can be derived with an accuracy of 1.4–2 m s^{-1} over an area of about 60 × 60 km (Fig. 12a). Figure 12b indicates that wind fields can indeed be observed when the reflectivity values are larger than both − 5 dBZ close to the receiver and 5 dBZ in an area with a radius of about 30 km around the transmitting radar. As a result, one can obtain measurements in the presence of light rain, stratiform and convective precipitation, and close to the receiver, even in some clear-air situations.

One can also determine wind information from outside the terminal area by using the DWD weather radar network (see Section 3.1). In addition to the monostatic and bistatic multiple-Doppler arrangements, the weather channel at Airport Surveillance Radars (ASRs), which measures reflectivity and, when upgraded, Doppler velocity, reinforces wind shear detection at airports.

During clear-air situations, the radar-based horizontal wind fields can be augmented by other sensors

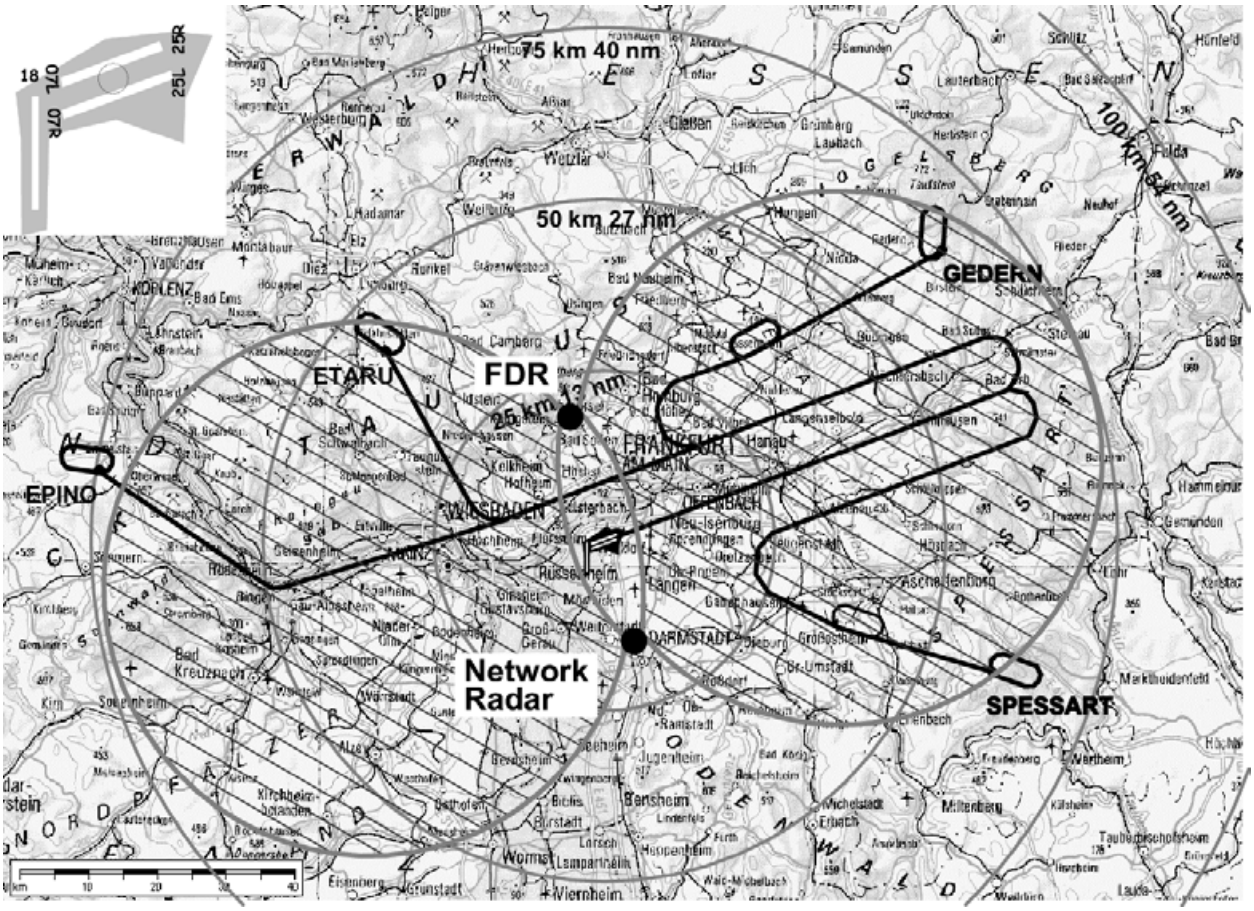

Figure 11. *Coverage of the terminal approach and departure area of the Frankfurt/Main International Airport showing a horizontal wind field using Doppler information extracted from both the monostatic Doppler radar within the DWD radar network (referred to as network radar) and the independent Frankfurt Doppler Radar (referred to as FDR). Horizontal wind fields within the aircraft arrival and departure areas can be determined using this hypothetical configuration. Thick lines indicate a sample for an approach to runway 25L or 25R. Runway location and runway code numbers are presented in the closeup view shown in the upper left-hand corner. The cross-hatched area indicates the dual-Doppler area with an intersecting angle limit of 20° and 160°.*

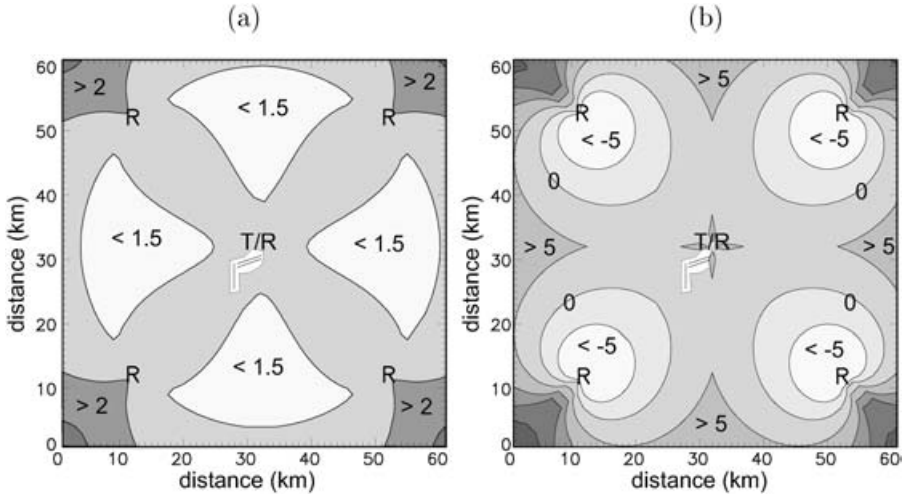

Figure 12. *Spatial distribution of (a) $\sigma^{bi}_{|V_b|}$ in m s^{-1} and (b) Z_{bmin} in dBZ is shown at ground level using an installation of four bistatic receivers grouped around the Doppler radar located at Frankfurt/Main International Airport.*

such as Doppler lidar systems or wind profilers, commercial airline data (so-called AMDAR data), and numerical forecast model output. How to integrate wind measurements with numerical model output is demonstrated in the ITWS terminal wind product described by Cole & Wilson (1994). The terminal wind product combines data from a local numerical weather prediction model together with observations made

from ground-based stations and radar systems in order to estimate horizontal wind fields within the three-dimensional space in the terminal area. When Doppler radar data become available, wind analysis is dominated by radar data. In other cases the three-dimensional wind field is based on the model output and other observations. A forecast is then achieved by using all the observations available for model initialisation.

4. Summary and recommendations

Both monostatic and bistatic multiple-Doppler radar networks are particularly well suited to deriving horizontal wind fields with high spatial and temporal resolutions over large areas during all precipitation events and, in some cases, in clear-air situations.

The advantages of using a monostatic dual-Doppler radar arrangement lie in its high sensitivity thanks to the use of pencil-beam antennas, the higher areal coverage from its scanning antenna, and a long-term experimental experience as compared to the use of bistatic Doppler radar systems with fixed broad-beam antennas. There are also uniquely scientific advantages in using a bistatic multiple-Doppler network rather than traditional monostatic dual-Doppler measurements, such as being able to measure simultaneously all the wind velocities for each individual resolution volume since there is only one source of illumination. Assuming a standard deviation in the horizontal wind of less than $3\ \mathrm{m\,s^{-1}}$ for monostatic and bistatic measurements, the areal coverage using bistatic dual-Doppler radar is about ten times smaller than that achieved with monostatic dual-Doppler radar. In the monostatic case, the area is limited by an intersecting angle varying between 20° and 160°, while in the bistatic case it is $25^\circ \leq \beta_b \leq 75^\circ$. However, since the cost of a bistatic receiver is less than 5% of a typical weather radar, the disadvantage can be minimised by installing a larger number of bistatic receivers with two antennas per receiver. In addition to the lower cost of purchase, installation requirements are also less for the bistatic than for monostatic radars. Because the bistatic system has only recently been developed, however, experimental experience has so far been confined to those four research institutes operating the bistatic multiple-Doppler radar network.

Choosing the best arrangement with the correct number of instruments should be based on the phenomena under investigation. Generally, for $\sigma_{|V_b|} \leq 3\ \mathrm{m\,s^{-1}}$ and a resolution on a Cartesian grid of below 1.5 km, the radar separation should range between 40 km to 80 km for a monostatic dual-Doppler arrangement (Davies-Jones 1979). Assuming the same standard deviation for a bistatic multiple-Doppler arrangement, the distance between transceiver and receiver should be of the order of 20 km and 30 km for $a_b = 150$ m, for $a_b = 300$ m between 40 km and 50 km, and for $a_b = 300$ m between 60 km and 70 km. However, it is important to bear in mind that as the distance from the radar increases, the vertical distance of the lowest detectable radar echo also increases.

The concept explained in Section 3.1 can be applied to each national or international weather radar network. The DWD covers nearly the entire country of Germany with Doppler weather radar measurements so that wind vectors can be estimated. In regions where more than one radar serves the same location, dual-Doppler techniques can be used for estimating wind vectors with an accuracy of $1.2\text{–}3\ \mathrm{m\,s^{-1}}$. However, the size of the areal coverage in which dual-Doppler techniques can be applied is small owing to of the long distance between radars. To improve the situation we recommend, therefore, either installing bistatic receivers to the already existing Doppler radars or applying single-Doppler wind techniques to derive horizontal winds from radial velocity. These options for enlarging an area of horizontal wind field retrieval are less expensive when compared with adding further monostatic Doppler radar systems to the existing radar network. When sufficiently developed, the single-Doppler techniques will be an important new source of determining horizontal wind vectors. Until such time, for those areas remaining and areas close to the ground, we recommend measuring using bistatic receivers.

The future for using horizontal wind fields for mesoscale applications such as nowcasting in the vicinity of airports lies in integrating all of the available observations within the area – e.g. mesonet stations, wind profilers, Doppler lidar systems, AMDAR data, low level wind shear alert systems – and combining them with a numerical weather prediction model. This integrated system can be based on either monostatic or bistatic radar. The Terminal Wind Product in the ITWS (Cole & Wilson 1994) gives a good example of how to analyse horizontal winds on a three-dimensional grid in the terminal area.

Acknowledgements

First, we would like to thank Jörg Seltman (German Weather Service, Hohenpeissenberg) and all the members of the DWD radar group for long and fruitful cooperation and data acquisition. Thanks also go to Nerissa Röhrs, who helped us with the English language. Parts of this study were supported financially by the BMVBW under contract L-1/2002-50.0294/2002 for which we also would like to express our thanks. Finally, we wish to acknowledge with thanks the constructive comments and changes suggested by the anonymous reviewers.

References

Bohne, R. A. & Srivastava, R. C. (1976) Random errors in wind and precipitation fall speed measurement by a triple

Doppler radar system. In *Proc. 17th Radar Meteorology Conf., Seattle*. Am. Meteor. Soc., 7–14.

Bougeault, P., Binder, P., Buzzi, A., Houze, R., Kuettner, J., Smith, R. B., Steinacker, R. & Volkert, H. (2001) The MAP Special Observing Period. *Bull Am. Meteorol. Soc*. 82: 433–462.

Bousquet, O. & Smull, B. F. (2003) Airflow and precipitation fields within deep alpine Valleys observed by airborne Doppler radar. *J. Appl. Meteor*. 42: 1497–1513.

Bringi, V. N. & Chandrasekar, V. (2001) *Polarimetric Doppler Weather Radar*. Cambridge, Cambridge University Press, 636 pp.

Browning, K. A. & Wexler, R. (1968) The determination of kinematic properties of a wind field using Doppler radar. *J. Appl. Meteorol*, 7: 105–113.

Carbone, R. E., Harris, F. I., Hildebrand, P. H., Kropfli, R. A., Miller, L. J., Moninger, W., Strauch, R. G., Doviak, R. J., Johnson, K. W., Nelosn, S. P., Ray, P. S. & Gilet, M. (1980) The multiple Doopler radar workshop, November 1979. *Bull. Am. Meteorol. Soc*. 61: 1169–1203.

Cole, R. E. & Wilson, F. W. (1994) The integrated terminal weather system terminal winds product. *The Lincoln Laboratory Journal*, 7: 475–502 (available at http://www.ll.mit.edu/AviationWeather/colewilson.pdf).

Davies-Jones, R. P. (1979) Dual-Doppler radar coverage area as a function of measurement accuracy and spatial resolution. *J. Appl. Meteorol*. 18: 1229–1233.

de Elia, R. & Zawadzki I. (2000) Sidelobe contamination in bistatic radars. *J. Atmos. Oceanic Technol*. 17: 1313–1329.

Doviak, J. R. & Zrnić, D. S. (1984) *Doppler Radar and Weather Observations*. Academic Press, Inc., 458 pp.

Easterbrook, C. C. (1975) Estimating horizontal wind fields by two-dimensional curve fitting of single Doppler radar measurements. In *16th Radar Meteorology Conf., Houston, TX. Am. Meteorol. Soc*., 214–219.

Friedrich, K. (2002) Determination of three-dimensional wind-vector fields using a bistatic Doppler radar network. PhD thesis, Fakultaet fuer Physik, Ludwig-Maximilians-Universitaet Muenchen, 135 pp. (available online at http://www.op.dlr.de/~pa4k/).

Friedrich, K. & Hagen, M. (2004) Wind synthesis and quality control of multiple-doppler-derived horizontal wind-fields. *J. Appl. Meteorol*. 43: 38–57.

Friedrich, K., Hagen, M. & Meischner, P. (2000) Vector wind field determination by bistatic multiple-Doopler radar. *Phys. Chem. Earth (B)* 25: 1205–1208.

Gerz, T. (2001) Wake vortex prediction and observation: towards and operational system. In *3rd ONERA-DLR Aerospace symposium ODAS 2001, Paris*, S1–3:1–10.

Hagen, M. (1989) Ableitung von Windfeldern aus Dopplermessungen eines Radars and Anwen-dung auf eine Kaltfront mit schmalem Regenband. PhD thesis, Fakultaet fuer Physik der Ludwig-Maximillians-Universitaet Muenchen, 108 pp.

Hagen, M., Friedrich, K. & Seltmann, J. (2002) Wind-field observation with the operational Doppler radar network in Germany. In *Proc. of the 2nd European Conference on Radar Meteorology, Delft, Netherlands*, 195–199.

Joss, J., Galli, G., Schaedler, B., Cavalli, R., Boscacci, M., Held, E., Bruna, G. D., Nespor, V. & Spiess, R. (1998) *Final Report NFP31: Operational Use of Radar for Precipitation Measurements in Switzerland*. Technical report, vdf Hochschulverlag AG an der ETH Zuerich (ISBN 3 72812501 6), 108 pp.

Laroche, S. & Zawadzki, I. (1994) A variational analysis method for retrieval of three-dimensional wind field from single-Doppler radar data. *J. Atmos. Sci*. 51: 2664–2682.

Lhermitte, R. M. & Atlas, D. (1961) Precipitation motion by pulse Doppler. In *Proc. 9th Weather Radar Conf., Bosten. Am. Meteorol. Sco.*, 498–503.

Lugauer, M., Berresheim, H., Corsmeier, U., Dabas, A., Dyck, W., Emeis, S., Egger, J., Fehr, T., Fiedler, F., Freuer, C., Gantner, L., Gilge, S., Heese, B., Hornsteiner, Hoeller, H., Jakobi, G., Junkermann, W., Kalthoff, N., Kaminski, U., Kirchner, M., Kraemer, H., Koehler, P., Kottmeier, C., Luksch, B., Plass-Duelmer, C., Reitebuch, O., Tagliazucca, M., Trickl, T., Vogt, S. & Winkler, P. (2003) An overview of the VERTIKATOR Project and results of alpine pumping. In *Preprints Int. Conf. on Alpine Meteorology, May 2003, Brigg*.

Miller, L. J. & Strauch, R. G. (1974) A dual Doppler radar method for the determination of wind velocities within precipitating weather systems. *Remote Sens. Environ*. 3: 219–235.

Persson, G. O. P. & Andersson, T. (1987) A real-time system for automatic single-Doppler wind field analysis. In *Proc. Symp. Mesoscale Analysis & Forecasting, Vancouver, Canada*, Volume SP-282, 61–66.

Protat, A. & Zawadzki, I. (1999) A variational method for real-time retrieval of three-dimensional wind field from multiple-Doppler bistatic radar network data. *J. Atmos. Oceanic Technol*. 16: 432–449.

Ray, P. S. & Sangren, K. L. (1983) Multiple-Doppler radar network design. *J. Climat. Appl. Meteorol.* 22: 1444–1454.

Ray, P. S., Stephens, J. J. & Johnson, K. W. (1979) Multiple-Doppler radar network design. *J. Appl. Meteorol.* 18: 706–710.

Ray, S. P., Wagner, K. K., Johnson, K. W., Stephens, J. J., Bumgarner, W. C. & Mueller, E. A. (1978) Triple-Doppler observations of a convective storm. *J. Appl. Meteorol*. 17: 1201–1212.

Ray, S. P., Ziegler, C. L., Bumgarner, W. & Serafin, R. J. (1980) Single- and multiple-Doppler radar observations of tornadic storms. *Mon. Wea. Rev*. 108: 1607–1625.

Satoh, S. & Wurman, J. (2003) Accuracy of wind fields observed by a bistatic Doppler radar network. *J. Atmos. Oceanic Technol*. 20: 1077–1091.

Schreiber, K.-J. (1998) Der Radarverbund des Deutschen Wetterdienstes. In *Annalen der Meteorologie 38: Herbst-schule Radarmeteorologie 1998*, 47–65. Deutscher Wetterdienst.

Skolnik, M. (1990) *Radar Handbook*. McGraw-Hill, Inc., 1200 pp.

Smythe, R. G. & Zrnić, D. S. (1983) Correlation analysis of Doppler radar data and retrieval of the horizontal wind. *J. Climat. Appl. Meteorol.* 22: 297–311.

Stoelinga, M. T., Hobbs, P. V., Mass, C. F., Locatelli, J. D. Bond, N. A., Colle, B. A., Houze, J. R. A. & Rangno, A. (2003) Improvement of Microphysical Prameterization through Observational Verification Experiment (IMPROVE). *Bull. Am. Meteorol. Soc*. 17: 1807–1826.

Sun, J., Flicker, D. W. & Lilly, D. K. (1991) Recovery of three-dimensional wind and temperature fields from simulated single-Doppler radar data. *J. Atmos. Sci*. 48: 876–890.

Takaya, Y. & Nakazato, M. (2002) Error estimation of the synthesized two-dimensional horizontal velocity in a bistatic Doppler radar system. *J. Atmos. Oceanic Technol*. 19: 74–79.

Tuttle, D. J. & Foote, G. B. (1990) Determination of the boundary layer airflow from a single Doppler radar. *J. Atmos. Oceanic Technol*. 7: 218–232.

Waldteufel, P. & Corbin, H. (1979) On the analysis of single-Doppler radar data. *J. Appl. Meteorol.* 18: 532–542.
Wurman, J. (1994a) Directly measured vector winds from an inexpensive bistatic multiple-Doppler radar network. In *COST75-Weather radar Systems*. Commission of European Communities, 562–573.
Wurman, J. (1994b) Vector winds from a single-transmitter bistatic dual-Doppler radar network. *Bull. Am. Meteorol. Soc.* 75(6): 983–994.
Wurman, J., Heckman, S. & Boccippio, D. (1993) A bistatic multiple-Doppler radar network. *J. Appl. Meteorol.* 32: 1802–1814.
Wurman, J., Randall, M., Frush, C. L., Loew, E. &Holloway, C. L. (1995) Design of a bistatic dual-Doppler radar for retrieving vector winds using one transmitter and a remote low-gain passive receiver. In *Proc. of the IEE—Special Issue on Remote Sensing Instruments for Environmental Research* 82: 1861–1872.
Zawadzki, I. (1973) Statistical properties of precipitation patterns. *J. Appl. Meteorol.* 12: 459–472.

A. Fundamentals

A.1. Principles of monostatic and bistatic measurements

Certain radar parameters such as range resolution, accuracy of Doppler velocity measurement, Nyquist velocity interval, and scattered power depend on the scattering angle, γ, which spans both the incident ray and the ray scattered towards the receiver (Table 3). Whereas those parameters are constant in the monostatic case due to $\gamma = 0$, $\cos(\gamma) = 1$, a high variability is observed in the bistatic case.

All signals arriving simultaneously at the receiver have the same travelling distance and form a surface of constant time delay. Within the bistatic radar system, surfaces of constant time delay between transmitted and received radar pulse are ellipsoids, with transmitter and receiver at the foci (Figure 1b). In the monostatic case, the surfaces of constant delay are spheres centred in the monostatic radar system (Figure 1a).

Whereas the length of sample volume in monostatic radar, a_t, is constant for a given pulse length, $c\tau$ with c being the speed of light and τ being the duration time, the length of bistatic sample volume, a_b, depends in addition on γ as illustrated in Table 3 and Figure 2 (de Elia & Zawadzki 2000; Friedrich 2002). The resolution achieved with the bistatic receiver is always inferior to that achieved by monostatic reception. Beyond the transmitter receiver baseline, b, $a_t/a_b = 1$. With increasing γ, a_t enlarges up to the length of the baseline ($a_b = b$), as illustrated in Figure 2 by a dashed, triple-dotted line.

In the case of monostatic radar, only those motions perpendicular to the spheres of constant delay (denoted as v_t) can be observed (Fig. 1a). For bistatic radar systems, these motions have to be perpendicular to the ellipsoids of contant delay, v_e (Protat & Zawadzki 1999). The standard deviation of the v_e measurement varies according to the scattering angle, as illustrated in Figure 2 by dashed and dotted line. For measurements within the area of $\gamma < 150°$, the standard deviation, σ_{v_e}, is less than 3 m s^{-1}, assuming a standard deviation of the wind measurements by a receiver of 0.8 m s^{-1}.

The Nyquist velocity interval (Table 3) depends on the wavelength λ, the sample time T_s (Doviak & Zrnić 1984), and the scattering angle γ. The Nyquist interval for monostatic radars, v_{nt}, is constant, whereas the Nyquist interval for bistatic reception, v_{ne}, depends also on γ. As a result, since $vne \geq vnt$, the bistatic Doppler velocity is folded less frequently (for more detail see Friedrich 2002).

A.2. Scattering characteristics

Bistatic scattering is a function of frequency, scatterer size, and scatterer shape as in the monostatic case, but it also depends in addition on the bistatic geometry itself. As a consequence, γ and the polarisation of both the incident wave and receiving antenna determine the amount of energy measured by the receiver. In

Table 3. *An overview of the radar configuration parameters of monostatic and bistatic Doppler radar systems. Each characteristic is explained in more detail in the text.*

	Monostatic radar	Bistatic radar
Scattering angle	$\gamma = 0°$	$0° \leq \gamma \leq 180°$
Surface of constant delay	Sphere	Ellipsoid
Sample volume length	$a_t = \frac{c\tau}{2}$	$a_b = \frac{c\tau}{2\cos^2(\gamma/2)}$
Velocity component	$v_t \perp$ Sphere	$v_e \perp$ Ellipsoid
Nyquist interval	$v_{nt} = \pm \frac{\lambda}{4 T_S}$	$v_{ne} = \pm \frac{\lambda}{8 T_S \cos(\gamma/2)}$
Scattering cross-section	$\sigma_{b\perp}(\mathrm{S},\mathrm{i}) = \sigma \sin^2(\varphi_t)$	$\sigma_{b\perp}(\mathrm{S},\mathrm{i}) = \sigma \sin^2(\chi)$
(Rayleigh scattering)	$\sigma_{b\parallel}(\mathrm{S},\mathrm{i}) = \sigma \cos^2(\varphi_t)$	$\sigma_{b\parallel}(\mathrm{S},\mathrm{i}) = \sigma \cos^2(\chi)\cos^2(\delta)$
Received power	$P_r \sim \frac{\sigma_b(\mathrm{S},\mathrm{i})}{r_t^2}$	$P_r \sim \frac{\sigma_b(\mathrm{S},\mathrm{i})}{r_b^2 \cos^2(\gamma/2)}$

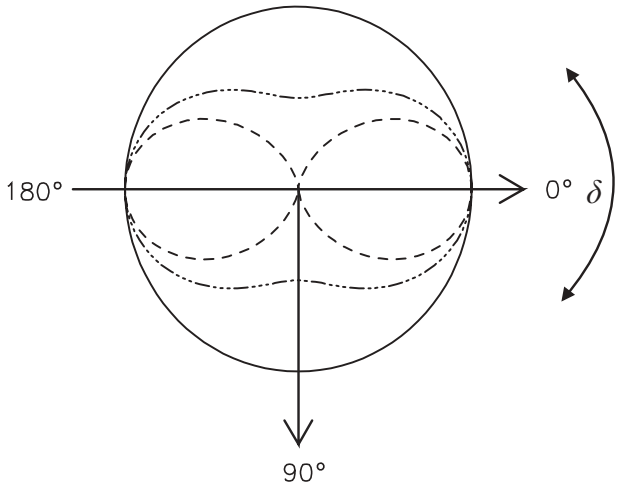

Figure 13. *Radiation diagram for Rayleigh scattering in the scattering plane. The radius vector to each curve is proportional to the intensity scattered at the corresponding forward scattering angle, δ. The solid line signifies the radiation pattern for polarisation transmitted vertically, the dashed line stands for transmitted horizontal polarisation, and the dotted-dashed line represents linear 45°/135° transmitted polarisation. The incident wave propagates from the left to the right. The particle's placement is in the centre.*

Table 3, the bistatic scattering cross-section, σ_b, is exhibited for Rayleigh scattering. The received intensity can then be further divided into a part perpendicular to the scattering plane ($\sigma_{b\perp}$) and another part parallel to the scattering plane ($\sigma_{b\parallel}$). Note that the polarisation of the receiving antenna specifies which part is measured. The unit vectors of the incident and scattered wave are denoted as $\mathbf{i}$ and $\mathbf{s}$, respectively. Figure 13 illustrates the radiation diagram for Rayleigh scattering.

In the monostatic case, the maximum intensity for linear polarisation is always received within the polarisation plane, i.e. for horizontal polarisation ($\varphi_t = 0°$), maximum energy is received within the horizontal plane (Figure 13). For bistatic reception, the received power, P_r, is affected by the forward scattering angle, δ with $\delta = \pi - \gamma$, and the polarisation angle, χ. The latter represents the transmitted polarisation angle and the rotation angle between the scattering plane and the plane facing towards the receiver ($\chi = \varphi_t + \omega$). Note that at ground level the rotation angle, ω, is zero. Detailed investigations on this topic can be found by de Elia & Zawadzki (2000), Bringi & Chandrasekar (2001) and Friedrich (2002). As demonstrated in Figure 13, the maximum energy can be received at ground level ($\omega = 0$) with vertically polarised transmission and reception. Investigations have shown that at higher elevations, slanted linear polarisation at 45° or 135° is favourable for transmitting in order to achieve a high backscattering signal at the vertically polarised bistatic antenna. The reason lies in the three-dimensional scattering process. While the transmitting and receiving planes are equal at ground level (Figure 13), they become intertwined at higher elevations.

As a consequence, both the bistatic resolution volume length and the dependency of the scattering cross section, $\sigma_b(\mathbf{s}, \mathbf{i})$, on the transmission and reception have to be considered within the radar equation. A general version of the radar equation of a beam-filling meteorological target can be written as

$$P_r = \frac{P_t G_t G_b(\phi_b, \theta_b) \lambda^2 \Delta\Phi_t \Delta\Theta_t a \sum_{vol} \sigma_b(\mathbf{s}, \mathbf{i})}{512 \pi^2 \ln(2) r^2}, \quad (7)$$

where P_t is the transmitted power, and G_t,G_b are the antenna gains of the monostatic and bistatic antennas, respectively; λ denotes the transmitted pulse's wavelength, and $\Delta\Phi_t$, $\Delta\Theta_t$ are the horizontal and vertical beamwidths of the transmitted pulse (de Elia & Zawadzki 2000). The resolution volume is denoted as a (see Table 3); $\sigma_b(\mathbf{s}, \mathbf{i})$ is the scattering cross-section; and r represents the distancae between target and receiver, which is r_b or r_t, respectively.

A.3. Optimal position of bistatic antenna

That area which can be observed by a broad-beam bistatic antenna is restricted by the receiving power pattern. Scanning receiving antennas, on the other hand, cannot track the transmitted pulses because they move at the speed of light. Therefore, it is important to consider not only the position of the receiver but also the bistatic antenna's viewing angle in order to achieve: (1) high spatial resolution of the measurement; (2) a high accuracy in the Doppler velocity measurement; (3) a low minimum detectable reflectivity factor, $Z_{b\min}$, measurable by the bistatic receiver; and (4) a high accuracy in the horizontal wind field determination based on the combination of v_e and v_t (Figure 2).

No Doppler velocity can be measured along the baseline ($\beta_b = 90°$) because of signal interferences. Close to the baseline, the length of a_b is of the order of several kilometres, and both σ_{v_e}, $\sigma^{bi}_{|V_b|}$ reach values higher than 10 m s^{-1} close to the baseline (Figure 2).

Beyond the transmitter receiver baseline, no independent wind components for horizontal wind vector estimation are measured (cf. Figure 2).

The area with β_b ranging between 25° and 75° provides measurements with standard deviations of the horizontal wind field of 2–3 m s^{-1} (for $\sigma_1 = \sigma_2 =$ 0.8 m s^{-1}), with a minimum at $\beta_b = 50°$ and a resolution volume length ranging between 180 and 1200 m (for $c\tau = 300$ m). Note that in this area the bistatic resolution volume is always larger than the monostatic

one. Received power depends on the distance r_b^2, the size of the resolution volume [$\sim \cos^{-2}(\gamma/2)$], and the three-dimensional scattering process of the transmitted wave [for Rayleigh scattering $I_\perp(\chi) \sim \sin^2(\chi)$]. Signals can be detected by a bistatic receiver when the reflectivity exceeds values of -5 dBZ at ground level and 5 dBZ at